Int. J. Nano Dimens., 13 (1): 96-104, Winter 2022

ORIGINAL ARTICLE

# The refractive index sensor of the SMF covered by nanodiamond layer

*Marzieh Nadafan[1,*], Javid Zamir Anvari[1], Azadeh Ahmadian[2], Zahra Reyhani Clor[1]*

[1] *Department of Physics, Faculty of Science, Shahid Rajaee Teacher Training University, Tehran, Iran*
[2] *Department of Physics, Faculty of Science, Tarbiat Modares University, Tehran, Iran*

Received 09 May 2021; revised 23 September 2021; accepted 25 September 2021; available online 02 October 202

**Abstract**

This study evaluated the light transmission characteristics of a single modular fiber with a cylindrical microchannel using the FDTD method. To this end, various microchannel diameters (4-11μm) were explored. The SMF included a silica core (n=1.4) coated by a nanodiamond layer with a refractive index of 2.42. The impact of Fabry-Perot resonance was evidently detected in transmission features. At constant λ, the light transmission variations depended on the refractive index of the microchannel. A significant change was observed in the upon altering the microchannel refractive index. Based on the results, a microchannel-based SMF with different diameters can be employed for refractive index sensing. In the cases where the diameter of the microchannel largely differs from that of the core (8μm), the transmission variations were negligible. The numerical results are in good agreement with those reported in the microhole or microchannel experiment. The highest and lowest transmissions were recorded for the microchannel at diameters of 4 and 11μm, respectively. Comparing related experimental and numerical results show proper control of the microchannel diameter can enhance light transmission through the core-microchannel. The sensitivity of the refractive index to the microchannel diameter is a promising feature that can be exploited for developing various fiber optical devices.

**Keywords:** *FDTD; Fiber Optics; Nanodiamond; Refractive Index; Sensors; Transmission.*

**How to cite this article**

*Nadafan M., Zamir Anvari J., Ahmadian A., Reyhani Clor Z. The refractive index sensor of the SMF covered by nanodiamond layer. Int. J. Nano Dimens., 2022; 13(1): 96-104.*

## INTRODUCTION

The application of the refractive index sensors has gradually increased in biological, chemical, and biomedical areas. In this regard, different methods have been explored to evaluate the refractive index. Owing to its compactness, light weight, and feasibility for in situ and/or remote assessments, fiber optic sensors have gained rising popularity [1, 2]. Moreover, the application of optical fiber provides the detections insensitive to electromagnetic interference [3]. In numerous in-fiber RI sensing systems, the transmission component can be conventional single-mode fibers (SMFs), polymer fiber, tapered fibers, and photonic crystal fibers (PCFs) possessing functional schemes such as fiber Bragg grating (FBG), long-period grating (LPG), and in-fiber interferometers [4-7].

Femtosecond lasers have been successfully used to write microchannels, as well as the ordinal SMFs and single-mode optical waveguides and micro-fluids in glass chips for refractive index sensing with improved features [8-10].

The index sensing features of these devices depend highly on the microchannel intersection structure [11]. The effect of scattering on a wavelength scale structure with high refractive index contrast has not been investigated in the intersection with a finite waveguide core in the

* Corresponding Author Email: *m.nadafan@sru.ac.ir*

fiber [12]. One of the methods that can be used to investigate the field passing through the optical fiber is to insert a microchannel into the fiber. Sometimes, a device should be inserted into the fiber, which should not be affected by the field or should be affected by the minimum field. In this paper, attempts were made to find the best location and characteristics of the microchannel for this purpose for refractive index sensing applications. Comparing the experimental results reported and numerical data validates the numerical method.

Here only the lower modes are supported by the waveguide because it is easier for waveguide to calculate the refractive index than others. The Pointing vector is calculated as 0.5 Real (E×H). This makes scattering density more useful in power transmission. Here the induced pulse is of Gaussian type with a central wave of 1550 nm in length and 200 fs in width, which is corresponding to a spectrum with 40nm thickness. In order to obtain and investigate the field, a monitor is placed within the microchannel that investigates the field inside the fiber and microchannel.

## OPTICAL FIBER SIMULATION: THEORY AND MODELLING

Optical fiber is indeed a cylindrical waveguide composed of two concentric cylinders called the core, with a larger refractive index ($n_1$) and a coating with a smaller refractive index ($n_2$). The fiber is made of two concentric cylinders with different diameters known as the core and the cladding. Core and cladding are made of dielectric materials while the refractive index of the cladding is lower than the refractive index of the core. A cylindrical microchannel intersecting fiber core is attracting more attention in the research field, especially in the application involving refractive index-related sensing.

Regarding the direction of wave propagation and the distribution of the lateral electric field in the light propagation direction, a 200μm cylinder was considered. Moreover, the core and cladding diameters of the fiber were set 8μm and 60μm, respectively. The microchannel was perpendicular to the light propagation direction. To observe the microchannel-guided wave propagation and the distribution of field along the propagation direction, a fiber length must be at least 200μm. Depending on the SMF on the fiber, the computation area can be confined to a rectangle (40μm□40μm) in the middle of which, the core was set. It should be noted that the scattering of the guided wave by a microchannel is a 3D problem but it was simplified to 2D one. This simplification will not reduce the accuracy of our calculation by the FDTD algorithm. In this simulation, the microchannel operates like a scatter in the core and a Fabry-Perot (FP) interferometer made of two concave mirrors. The refractive index of the core and its surroundings determined the reflectivity.

Herein, the 2D scattering problem examined using an FDTD method, in which TE polarization (Hx, Ey, Hz) is taken into account. Additionally, the Ey component is normal to the paper (i.e it is along the micro-channel). The core width is also taken as 8μm. For the core-cladding index difference of 0.003 ($n_{cladding}$=2.42, $n_{core}$=2.423), the waveguide could support the lowest mode only. For attaining transmission spectrum data from the FDTD simulations, pulse excitation could be included in FDTD iteration rather than CW excitation. Fig. 1 (a, b) represent the SMF based on a microchannel and the cross section of computation area of SMF with core, cladding and microchannel parts. Table 1 shows the exact value of parameters used in modelling procedure.

## RESULTS AND DISCUSSION

*The scattering of electric field distribution*

A CW light at 1550nm with 200fs width was used for simulation of scattering wave of the fiber by a microchannel in different diameters (4, 6, 8, and11 μ m). The refractive index of microchannel

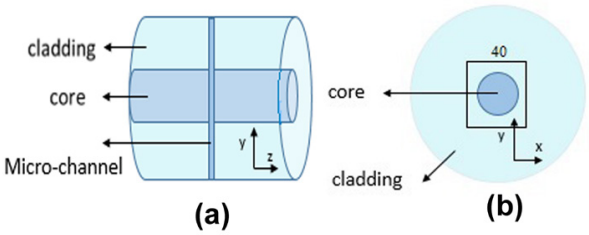


Fig. 1. (a) Schematic diagram of a microchannel passing through the core of an SMF, (b) cross-section of computation area of SMF with core, and cladding parts.

($n_h$) changed from 1.0 to 1.4 with 0.1 step.

The longitudinal Poynting vector distribution pattern from 4, 6, 8 and 11μm microchannel fiber sensors have been provided with refractive index of 1.0 for (a), (b); 1.2 for (c), (d); 1.4 for (e), (f) in Figs. 2-5, respectively. The (a), (c), and (e) parts in Figs. 2-5 are the enlarged field distribution near the microchannel radius. The (b), (d), and (f) parts in Figs. 2-5 show the transmission pattern from the microchannel to about 20μm away from the center of microchannel. The same color bar has been shown on the right.

According to Figs. 2-5, the observable scattering wave and re-coupling the scattered wave related to the refractive index. The transmitted light into the fiber changes nonlinearly with $n_h$. It should be noted that the transmission of fiber depended on the microchannel structure and the light wavelength. In fact, the light transmitted through the fiber has a nonlinear response in terms of the refractive index of the microchannel.

Mostly, the light emitted by the waveguide is dispersed after being scattered in the fiber core of the microchannel. The light returned to the core provided the conditions for the total internal reflection and phase matching at the core-cladding boundary which can be assigned to both roles of FP cavity (scattering, reflecting). The variation of the refractive index in the microchannel not only varies the reflectance of the core-channel boundary but also alters the optical pathway between two mirrors. Changing in the optical pathway is directly related to the resonance wavelength of the FP cavity.

By increasing refractive index, the electric transient field at the center(x=0) increases (the red color rate has increased). On the other hand, the intensity of green color has increased at this point indicating the increased rate of transient field. As it can be observed in the figure, at radius 2μm, which is the boundary between the microchannel and the core, the field gets stronger as the

Table 1. The values of parameters used in the modelling of SMF.

| Parameter | Value |
|---|---|
| $n_{cladding}$ | 2.42 |
| $n_{core}$ | 2.423 |
| L (length fiber) | at least 200 μm |
| core diameter | 4, 6, 8, and 11 μm |
| cladding diameter | 60 μm |
| $n_{Microchannel}$ | 1, 1.1, 1.2, 1.3, and 1.4 |
| computation area (square) | 40μm×40μm |

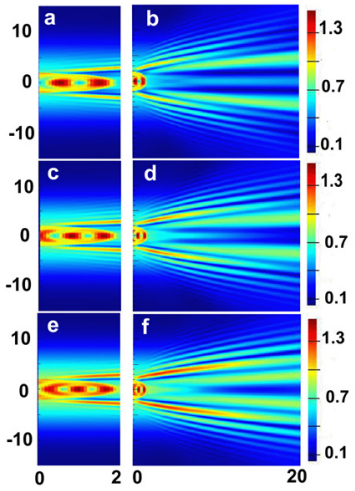


Fig. 2. $E_y$ field distribution of the guided wave scattered by the microchannel with 4 μm diameter with different refractive index of (a) and (b) n=1, (c) and (d) n=1.2, (e) and (f) n=1.4. The transverse fields passing through 20 μm are shown in (b), (d), and (f). (a), (c), and (e) show the transverse fields passing through 2 μm.

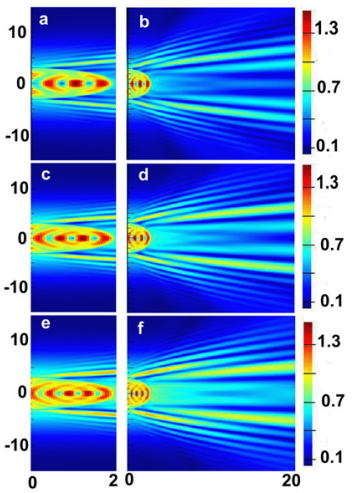


Fig. 3. $E_y$ field distribution of the guided wave scattered by the microchannel with 6 μm diameter with different refractive index of (a) and (b) n=1, (c) and (d) n=1.2, (e) and (f) n=1.4. The transverse fields passing through 20 μm are shown in (b), (d), and (f). (a), (c), and (e) show the transverse fields passing through 2 μm.

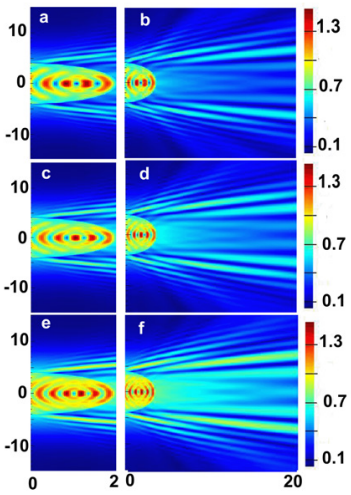


Fig. 4. $E_y$ field distribution of the guided wave scattered by the microchannel with 8 μ m diameter with different refractive index of (a) and (b) n=1, (c) and (d) n=1.2, (e) and (f) n=1.4. The transverse fields passing through 20 μ m are shown in (b), (d), and (f). (a), (c), and (e) show the transverse fields passing through 2 μ m.

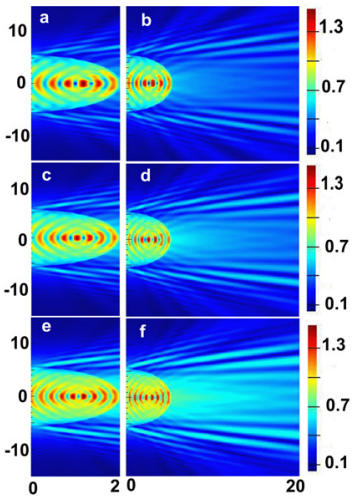


Fig. 5. $E_y$ field distribution of the guided wave scattered by the microchannel with 11 μ m diameter with different refractive index of (a) and (b) n=1, (c) and (d) n=1.2, (e) and (f) n=1.4. The transverse fields passing through 20 μ m are shown in (b), (d), and (f). (a), (c), and (e) show the transverse fields passing through 2 μ m.

refractive index increases. This indicates that the transient light is better reflected in exposure to microchannel and a stronger field is created. The greater the refractive index, the higher the intensity of transient field from microchannel to pass it and reentering the core; and the higher intensity of the light that exits the microchannel, enters the core, and goes on(along the y-axis).

From the results obtained in the microchannel diameter that is equal to the core, an increase in the refractive index has caused an increase in the field inside the microchannel and the scattering rate increases at each stage. On the other hand, by increasing the refractive index, the light exits the microchannel with further changes and the field gets stronger while going on along its path in the fiber.

Because of the FP resonance effect in the microchannel, a significant transmission variation is expected in the incident light upon altering the microchannel refractive index, which could be exploited in high-resolution index sensing.

*Transmission properties of the microchannels with various diameters*

According to Figs. 6 and 7, the transmission highly depended on the index while its dependence on the wavelength was negligible. Figs. 6 (a, b, c and d) represents the transmission dependence on the microchannel refractive index for various wavelengths. The transmission vividly changed with the refractive index of the microchannel spatially for 6-8 μm diameter of microchannel. The changes in the transmission got more observable in 8μm diameter of the microchannel. When the microchannel diameter was far different from the core diameter (8 μm), the transmission changes were not noticeable. Herein, the highest and lowest values of the whole transmission belonged to the microchannels with respective diameters of 4 μm and 11 μm; regardless of the wavelength. However, the overall transmittance has the smallest value for the smallest microchannel. It is obvious when increasing the refractive index of the microchannel, the recorded transmission decreased. Decreasing transmittance is independent of the wavelength of incident light. According to experimental results reported, turning 3D to 2D and estimation about resolution of refractive index are confirmed our numerical results [13].

As mentioned before, the microchannel is similar to an FP cavity as it is dependent on the light wavelength. Small alternations were observed in the transmission due to the inferior reflectivity of the core-microchannel boundary. Nonetheless, the free spectral range of the FP cavity was bigger than the wavelength changes. Thus, different wavelengths will exhibit similar behaviors by the

refractive index changes in a microchannel with different diameters Figs. 7 (a, b, c and d). Therefore, the transmitted light decreased by increasing the refractive index of the microchannel.

The obtained results are in line with the previous reports [13, 14]. Qui et al. simulated the SMF in microchannels, in which the refractive index of the core material was 1.4 while in the present study, it is 2.42 [15]. Qui and his coworkers claimed the microchannel diameter in the range of 4-6µm is the most adequate size for optimizing the transmission [15]. In this study, the transmission of the microchannel with diameters of 6, and 8µm showed similar behavior as reported before [15]. Recently, an SMF-based micro-hole was also fabricated (by femtosecond laser) and simulated whose results are in agreement with our findings [16]. Their experimental and numerical results showed the nonlinear transmission of this microhole which coincided with our findings in the nonlinear behavior of microchannel.

*Transmission properties for different microchannel diameters*

The index-sensing capability of the developed microchannel devices was further examined for $\lambda = 1550$nm. First, the transmission properties of microchannel with diameters of 6, 8, and 11µm were numerically assessed at $\lambda = 1550$nm and compared with the empirical findings of previous reports as presented in Fig. 8 [8, 15-16]. For various microchannel diameters, the determined transmission ranged from -5.8dB to -10.2dB in the refractive index interval of 1.0 –1.4. These results are in properly consistent with the empirical reports in the refractive index range of 1.30-1.37 [16]. According to Zhou et al. reports, the obtained results of the larger microchannel diameter are much agreement with our numerical results than the results of the smaller microchannel diameters [16]. It could be drawn that on the range 1.05 to 1.15 the microchannel with 6µm diameter has the lowest transmission loss than other microchannels. However, the microchannel with 8µm diameter has the best transmission on the range of 1.17 to 1.23. Comparison among these microchannels results shows that the diameter of microchannel is about 6µm, whose lowest loss in middle range of refractive index, and the 4µm diameter microchannel, whose lowest loss at the beginning and end of interval refractive index, are more suitable for sensing application.

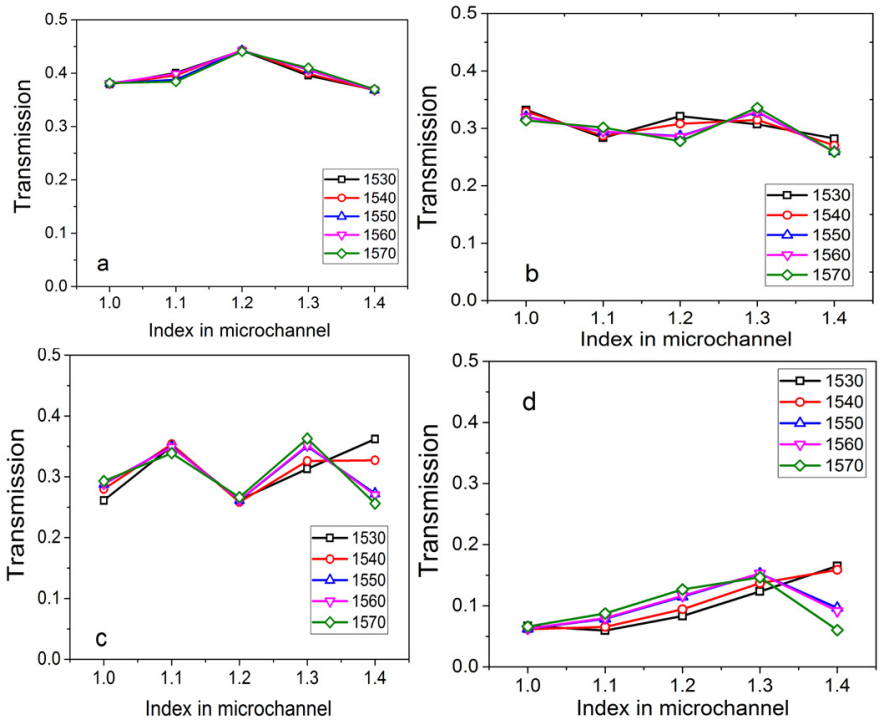


Fig. 6. The dependence of the transmission on the refractive index in a cross-sectional of (a) 4µm, (b) 6µm, (c) 8µm, and (d) 11µm microchannel diameter for different wavelength.

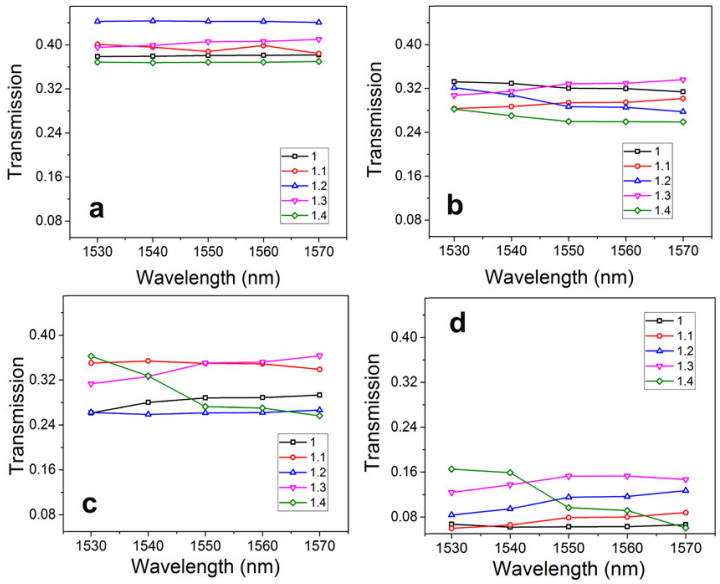


Fig. 7. The dependence of the transmission versus different wavelengths for (a) 4µm, (b) 6µm, (c) 8µm, and (d) 11µm microchannel diameter for different refractive index of microchannel.

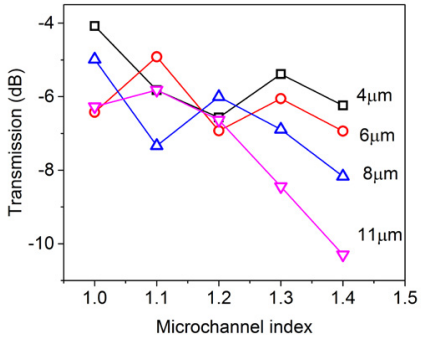


Fig. 8. Calculated transmission properties for microchannel diameters of 4µm, 6µm, 8µm, and 11µm.

For 11µm microchannel, the simulation results of transmission properties do not show any refractive index turning point unlike the other three diameters of microchannel. The reason of existing some differences between our numerical findings and the Zhou's reports is related to the difference between the shape and the roughness of the microchannels [16]. According to Fig. 9, the slope of transmission vs. refractive index is completely in good agreement with the experimental results of 25 dB/RIU reported in Ref. [14] of 33 dB/RIU, which are close to experimental results and validate the numerical simplification method.

The transmission properties showed the dependence of transmittance with respect to microchannel index for different microchannel diameters. Figs. 9 (a, b, c and d) illustrates the periodical fluctuation with incrementing the refractive index. Despite uneven fluctuation amplitudes, the period declined by raising the microchannel diameter, which has been resembled the features of a typical FP cavity. A typical FP cavity includes 2 flat mirrors and its overall transmittance can be easily determined as [17]:

$$T_i = \frac{(1-R)^2}{(1-R)^2 + 4R\,\mathrm{Sin}^2\left(\frac{2\pi}{\lambda} nh\right)} \quad (1)$$

in which, h shows the cavity length, n denotes the refractive index of the FP cavity, and R

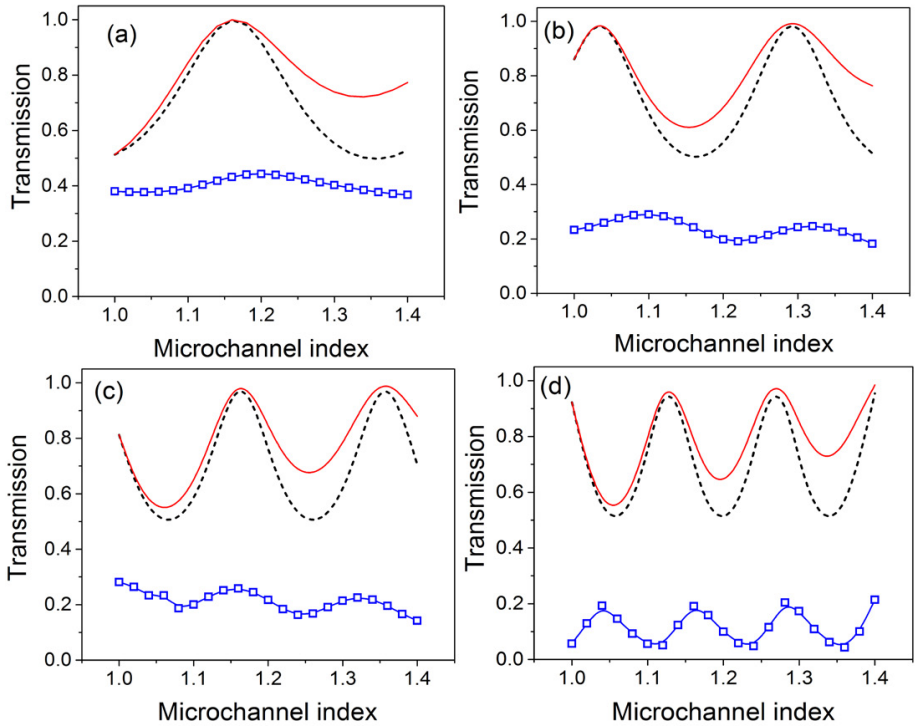


Fig. 9. Calculated transmission properties of SMF-based microchannel device for (a) 4µm, (b) 6µm, (c) 8µm, and (d) 11µm microchannel diameters; the dash line represents the transmission properties of a typical FP cavity with different cavity lengths (h = d/2) filled with air; the solid line represents the transmission properties of a typical FP cavity with different cavity lengths (h = d/2) filled with different refractive indices (n=1, 1.1, 1.2, 1.3 and 1.4).

represents the reflectivity of the mirrors. The period of transmission fluctuation vs. refractive index of an SMF-based microchannel device with a microchannel diameter of d was close to that of a typical FP cavity with a cavity length of h=d/2. Based on previous studies, the scattering effect can also influence the transmission characteristics, resulting in several interesting features other than an FP cavity. For instance, the overall transmittance will be higher when the diameter of the microchannel largely differs from that of the core. Large microchannel diameter causes to the small transmittance. By increasing the microchannel diameter, the range of transmittance is decreased. The guided light is angularly dispersed upon scattering by the microchannel. The angular distribution of the scattered light highly depends on the microchannel refractive index as extensively explored and analyzed in Ref. [8, 16].

Concerning ray optics, the incident light is repeatedly refracted at the core-microchannel interface and the exit angle of the refracted light alters by the microchannel index. The refracted light rays satisfying total internal reflection can be re-guided.

The high-resolution refractive index sensing requires a significant linear variation of transmission with the microchannel refractive index in a broad index range. For small microchannel diameters (e.g. 4µm), the transmission variations with the refractive index are slow. For larger microchannels (d=11µm), however, the entire transmission is quite small. It maybe for the reason of large and weak scattering, it showed in big and small microchannel diameters, respectively [16]. The accessible index range for sensing purposes is also narrow since the FP resonance-induced fluctuation period declines with the elevation of the microchannel diameter. Based on the literature, both scattering and FP resonance effects play a decisive role in the intermediate microchannel diameters (6–8 µm). The optimum microchannel diameter was ~6 µm. The high index sensing capability is related to microchannel of 6µm in diameter in the index range of 1.00–1.10, 1.10–1.20, 1.20-1.30 and 1.30–1.40. Lai *et al.* discussed experimentally about the optimal choice of microchannel radius is around 4-6µm, in which

Table 2. The comparison among obtained simulated results and similar other works.

| No. | λ(nm) | $n_{microchannel}$ | shape | Microchannel Diameter (μm) | Transmittance | Ref. |
|---|---|---|---|---|---|---|
| 1 | 1550 | 1.3 | Cylindrical microhole | 4 | -7 (dB) | [15] |
| 2 | 1550 | 1.3 | Cylindrical microhole | 6 | -17 (dB) | [15] |
| 3 | 1550 | 1.3 | Cylindrical microhole | 8 | -5 (dB) | [15] |
| 4 | 1550 | 1.3 | Cylindrical microhole | 11 | -3 (dB) | [15] |
| 5 | 1550 | 1.3 | Taper microhole | 6 | -10 (dB) | [16] |
| 6 | 1550 | 1.3 | Cylindrical microhole | 6 | -10 (dB) | [16] |
| 5 | 1550 | 1.3 | Taper microhole | 8 | -3 (dB) | [16] |
| 6 | 1550 | 1.3 | Cylindrical microhole | 8 | -4 (dB) | [16] |
| 5 | 1550 | 1.3 | Taper microhole | 11 | -2 (dB) | [16] |
| 6 | 1550 | 1.3 | Cylindrical microhole | 11 | -3 (dB) | [16] |
| 7 | 1550 | 1.3 | Cylindrical microhole | 4 | -5.5 (dB) | Here |
| 8 | 1550 | 1.3 | Cylindrical microhole | 6 | -6 (dB) | Here |
| 9 | 1550 | 1.3 | Cylindrical microhole | 8 | -7 (dB) | Here |
| 10 | 1550 | 1.3 | Cylindrical microhole | 11 | -10.5 (dB) | Here |

6μm microchannel revealed high refractive index sensing that is confirmed the numerical results completely [13]. Table 2 represent the normal comparison among obtained simulated results and similar other works that are pointed before. The SMF-based microchannels are is promising candidates as they offer larger transmission variations in an appropriate refractive index range.

## CONCLUSION

The current research is devoted to simulating a CNS-coated SMF with a microchannel intersecting the core. The FDTD (2D) method was employed to determine the numerical results. The calculated transmission vs. refractive index of microchannel shows good agreement with reported experimental results, which confirms and validates this research. Various transmission properties were observed in microchannels with different diameters (from 4 to 11 μm) within the refractive index range of 1.0 to 1.4. A decline was seen in the transmitted light upon enhancing the microchannel refractive index. In the case of the core of SMF possessing the diameter of 8μm, the microchannel demonstrated the highest variations in transmission. The transmission findings also suggested the significant role of the FP resonance in the transmission features. A simple core-microchannel structure can be employed for refractive index sensing owing to its well-controllable diameter as the diameter size can dramatically affect the transmission rate in the optical fibers.

## ACKNOWLEDGEMENT

The work was supported by Shahid Rajaee Teacher Training University under contact number 000118.

## CONFLICT OF INTEREST

Authors have no conflict of interest

## REFERENCES

[1] Beitollahi H., Safaei M., Tajik S., (2019), Application of Graphene and Graphene Oxide for modification of electrochemical sensors and biosensors: A review. *Int. J. Nano Dimens.* 10: 125-140.

[2] Girigoswami K., Akhtar N., (2019), Nanobiosensors and fluorescence based biosensors: An overview. *Int. J. Nano Dimens.* 10: 1-17.

[3] Tariyal B. K., Cherin, A. H., (2003), Optical fiber communications. In R. Meyers (Ed.), *Encyclopedia of Physical Science and Technology*.

[4] Tian Y., Wang W., Wu N., Zou X., Wang X., (2011), Tapered optical fiber sensor for label-free detection of biomolecules. *Sensors*. 11: 3780-3790.

[5] Yousefi E., Hatami M., (2020), A numerical method for pulse propagation in nonlinear fiber Bragg grating with ternary stability nature. *Opt. Fiber Technol.* 54: 102075.

[6] Garg R., Tripathi S. M., Thyagarajan K., Bock W. J., (2013), Long period fiber grating based temperature-compensated high performance sensor for bio-chemical sensing applications. *Sens. Actuators B.* 176: 1121-1127.

[7] Lu P., Men L., Sooley K., Chen Q., (2009), Tapered fiber Mach–Zehnder interferometer for simultaneous measurement of refractive index and temperature. *Appl. Phys. Lett.* 94: 131110.

[8] Wang Y., Wang D. N., Yang M. W., Hong W., Lu P., (2009), Refractive index sensor based on a microhole in single-mode fiber created by the use of femtosecond laser micromachining. *Optik*. 34: 3328-3330.

[9] Mou C., Zhou K., Davies E., Zhang L., Bennion I., (2009), Fiber laser incorporating an intracavity microchannel for refractive index and temperature sensing. *Photon. Technol. Lett.* 21: 1559–1561.

[10] Wei T., Han Y., Tsai H. L., Xiao H., (2008), Miniaturized fiber inline Fabry–Perot interferometer fabricated with a femtosecond laser. *Opt. Lett.* 33: 536–538.

[11] Ran Z. L., Rao Y. J., Liu W. J., Liao X., Chiang K. S., (2008), Laser-micromachined Fabry–Perot optical fiber tip sensor for high-resolution temperature-independent measurement of refractive index. *Opt. Exp.* 16: 2252-

2263.
[12] Sun H., He F., Zhou Z., Cheng Y., Xu Z., Sugioka K., Midorikawa K., (2007), Fabrication of microfluidic optical waveguides on glass chips with femtosecond laser pulses. *Opt. Lett.* 32: 1536–1538.
[13] Lai Y., Zhou K., Zhang L., Bennion I., (2006), Microchannels in conventional single-mode fibers. *Opt. Lett.* 31: 2559-2561.
[14] Petrovic J., Lai Y., Bennion I., (2008), Numerical and experimental study of microfluidic devices in step-index optical fibers. *Appl. Opt.* 47: 1410-1416.
[15] Qiu J., Hong W., Wang D. N., Gao D., Wang Y., Li Y., (2011), Transmission properties of the single mode fiber with a cross-sectional micro-channel investigated using time-domain finite difference (FDTD) method. *Opt. Fiber Technol.* 17: 580-585.
[16] Zhou J., Zheng Y., (2019), Fiber refractive index sensor with lateral-offset micro-hole fabricated by femtosecond laser. *Optik.* 185: 1-7.
[17] Yariv A., Yeh P., (2007), *Optical electronics in modern communications.* Oxford University Press.